JOURNAL OF PROPULSION AND POWER
Vol. 21, No. 5, September–October 2005

# New Aluminum Agglomeration Models and Their Use in Solid-Propellant-Rocket Simulations

T. L. Jackson,* F. Najjar,† and J. Buckmaster‡
*University of Illinois at Urbana–Champaign, Urbana, Illinois 61801*

**Random packs of ammonium perchlorate and aluminum particles in fuel binder, of the kind used to mimic the morphology of heterogeneous propellants, define distributions of aluminum particles that can be used as the starting point of agglomeration studies. The goal is to predict the fraction of aluminum that agglomerates and the size distribution of the agglomerates. Three phenomenological models are described, each with one or two parameters that can be adjusted to fit experimental data, and a number of such fits are attempted. It is shown that the agglomeration models can be calibrated to match a wide variety of propellant outputs, as needed for the numerical simulation of rocket chamber flows with aluminum injection. Results for such flows are presented and provide information about the distribution of the aluminum droplets and of the alumina smoke particles that arise from its presence.**

## I. Introduction

TYPICAL solid-rocket-motor propellants, such as those used in the space shuttle boosters, are composed of ammonium perchlorate (AP) and aluminum (Al) particles embedded in a fuel binder. A typical composition, by weight, is 71% AP, 18% Al, and 11% binder. The aluminum reacts exothermically with $H_2O$ and $CO_2$ in the chamber, increasing the specific impulse by approximately 10%. It also provides efficient damping of chamber instabilities, a desirable effect. However, there are undesirable effects such as slag accumulation, nozzle erosion, and significant exhaust signatures. Because of these, aluminum behavior is one of the most important problems faced by the solid-propellant-rocket industry.

Whole system numerical rocket simulations are not able to resolve the details of the combustion field or the individual Al particles, and so they need as a boundary condition the statistics of the aluminum flux at the edge of the combustion field, the total number flux, and the particle size probability density function (PDF). Such injection data can either be defined by an extensive experimental database or by a combination of theory and empirical data.

A detailed summary of the history of aluminum particles originating within the propellant and passing into the chamber can be found in Ref. 1. Each particle, typically 5–40 $\mu$m in diameter, arrives individually at the surface. There follows a residency period during which the particle can move over the surface and agglomeration with other particles can occur. Other propellant ingredients can be entrained within the agglomerate. Whether or not agglomeration occurs, the aluminum particles eventually lift from the surface and enter the high-temperature chamber where combustion occurs. Burn-up takes place at a large distance from the surface.

The actual process of agglomeration is complex, and the ingredients favorable for it are poorly known. Controlling parameters include the binder type and amount, the oxidizer size and size distribution, the thickness of the surface melt layer, the aluminum size and size distribution, the details of the nonplanar surface regression, the surface residence time of the aluminum, the chamber pressure, etc. A single agglomeration, after detachment from the surface, is a spherical globule with a diameter that can be as large as hundreds of microns.

In principle, it should be possible to predict the agglomeration details via a full simulation of the propellant combustion. Simulation of nonaluminized propellant burning is possible using a code that we call Rocfire,[2] and recently the injection of isolated aluminum particles has been included within that framework.[3,4] However, further progress is hampered by the limits on computational resources and a lack of adequate models for various components of the physics.

Past work is predominantly empirical in nature, a matter of curve fitting. Typically, the input parameters are a subset of those that characterize the propellant morphology. For example, for a bimodal propellant (coarse and fine oxidizer) with aluminum particles of a single size, these parameters could include $D_{\mathrm{ox},c}$ the diameter of the coarse oxidizer particles and $F$ their weight fraction; $D_{\mathrm{ox},f}$ the diameter of the fine oxidizer particles and $C$ their weight fraction; $T = F + C$ the total weight fraction of oxidizer; and $D_{\mathrm{Al}}$ the diameter of the aluminum particles. Thus Beckstead,[5] in analyzing an Aerojet database, proposed the formula

$$A_0 = 0.0005 D_{\mathrm{ox,C}}\, D_{\mathrm{Al}}^{\frac{1}{4}} \left[ \frac{1 + 30(F/C)}{1 + 80(F/C)^2} \right] \tag{1}$$

for $A_0$ the agglomeration fraction (the fraction of aluminum that has agglomerated). And Cohen and Strand[6] used the same data but proposed the formula

$$A_1 = (F/T)\{[0.38 \log(D_{\mathrm{ox,C}}) - 1.61](D_{\mathrm{ox,F}}/40) - 0.96 \log(D_{\mathrm{ox,C}}) + 4.13\}$$

$$A_0 = A_1 + 0.479 \log(D_{\mathrm{ox,C}}) + (D_{\mathrm{ox,F}}/100)[2.01 - 0.48 \log(D_{\mathrm{ox,C}})] - 1.964 \tag{2}$$

Formulas of this kind can have value in design strategies of course, particularly when extended to account for pressure variations or aluminum size distributions.[6] A key failing, however, is that they say nothing about the size distribution of the agglomerates, and yet it is this distribution that is of fundamental importance in the examination of, say, nozzle erosion; for only particles greater than some critical size impinge on the nozzle wall and contribute to the erosion.

Another flaw of such formulas is that they are not linked to any of the physics that controls agglomeration, and so there is no path to

Received 29 June 2004; presented as Paper 2004-4042 at the AIAA/ASME/SAE/ASEE 40th Joint Propulsion Conference and Exhibit, Fort Lauderdale, FL, 11–14 July 2004; revision received 6 January 2005; accepted for publication 10 January 2005. 

*Senior Research Scientist, Center for Simulation of Advanced Rockets. Senior Member AIAA.

†Senior Research Scientist, Center for Simulation of Advanced Rockets. Member AIAA.

‡Professor, Department of Aerospace Engineering; limey@uiuc.edu. Associate Fellow AIAA.

improvement or enrichment, nor the hope that assigned parameters might be derived from modeling.

In the strategy that we shall describe in this paper, the propellant morphology is accounted for by the use of three-dimensional models generated by a random-packing algorithm, something not hitherto attempted. In this sense, all morphology parameters are accounted for. The agglomerate size distribution arises from the model in a natural way.

The only previous modeling attempt that we are aware of is from Cohen.[7] He assumes that the largest AP particles are represented by a uniform distribution of spheres in a cubic array, with pockets between them. These pockets are filled with binder, fine AP particles, and aluminum particles, and it is assumed that each agglomerate is made up of the fraction of aluminum that melts within each pocket. A key observation is that large particles will not melt upon passage through the thermal layer of the propellant and so cannot agglomerate, whereas small particles will melt: the critical melt diameter is estimated to be

$$D_{\text{melt}} = \left[ \frac{12\lambda_b \kappa_b}{\rho_{\text{Al}} c_{\text{Al}} r_b^2} \left( \frac{T_s - T_m}{T_m - T_0} \right) \right]^{\frac{1}{2}} \tag{3}$$

where $\lambda_b$ is the binder thermal conductivity, $\kappa_b = \lambda_b/(c_b \rho_b)$ is its diffusivity, $\rho_b$ its density, $c_b$ its specific heat, $\rho_{\text{Al}}$ is the aluminum density, $c_{\text{Al}}$ its specific heat, $r_b$ is the burn rate, $T_s$ the surface temperature, $T_m$ the aluminum melting temperature, and $T_0$ the supply temperature. [Cohen presents no derivation of this result, but it proceeds as follows: assume that the heat flux per unit area per unit time to a particle of diameter $D$ is $\lambda_b(T_s - T_m)2/D$ and the total heat flux during transit through the thermal layer is obtained by multiplying this by the area $\pi D^2$ and the transit time $\lambda_b/\rho_b c_b r_b^2$. This is equated to the change of thermal energy of the particle $\rho_{\text{Al}} c_{\text{Al}}(T_m - T_0)\pi D^3/6$.] It is only necessary then to know the fraction of aluminum defined by particles of diameter less than $D_{\text{melt}}$ in order to determine the size of each agglomerate and the agglomeration fraction. Because a size distribution is not predicted, the predicted size defines a mean value. In summary, near neighbors (here those within a single pocket), if they melt, will agglomerate.

The concept of near neighbors is a sensible one. Particles that are well separated horizontally (parallel to the surface) will not agglomerate because their horizontal migration at the surface is bounded during the finite residence times. And particles that are well separated vertically will not agglomerate because the upper one will detach from the surface before the lower one reaches it. What is uncertain, of course, is the shape and size of the domain occupied by each particle's nearest neighbors, the agglomeration domain. Fundamentally, the pocket model assumes that the agglomeration domain for each particle in a pocket contains only the other particles in that pocket and none of those in other pockets.

A necessary (but not sufficient) condition for this to be true is that the pockets are sharply defined, and this is something that can be examined using the packing algorithm that we have used in our propellant combustion modeling. It is described in Refs. 8 and 9. Figure 1a shows an example of a 10,000 particle pack of coarse AP, fine AP, and aluminum, and Fig. 1b shows just the aluminum particles in the pack. Although there are some clusters of aluminum that are, roughly speaking, isolated, it is clear that this is not a general characteristic. And indeed, this is consistent with experimental observations of random packs reported in Ref. 10 in which agglomerates much larger than those predicted by the pocket model are reported.

In the strategy that we shall describe in this paper, the concept of an agglomeration neighborhood will be used, with parameters that at the present time can only be defined empirically. For the simplest model there is only a single parameter, and of course this can be chosen so that the agglomeration fraction is matched, or the mean agglomerate size is matched. However, the model also yields a description of the agglomerate size distribution, and so, in this important sense, is predictive. In addition, for situations where variations of the agglomeration fraction with some parameter (pressure say) are known experimentally, the functional dependence of the agglomeration domain parameter can be chosen to match the variations. This provides an alternative to formulas such as Eqs. (1) and (2).

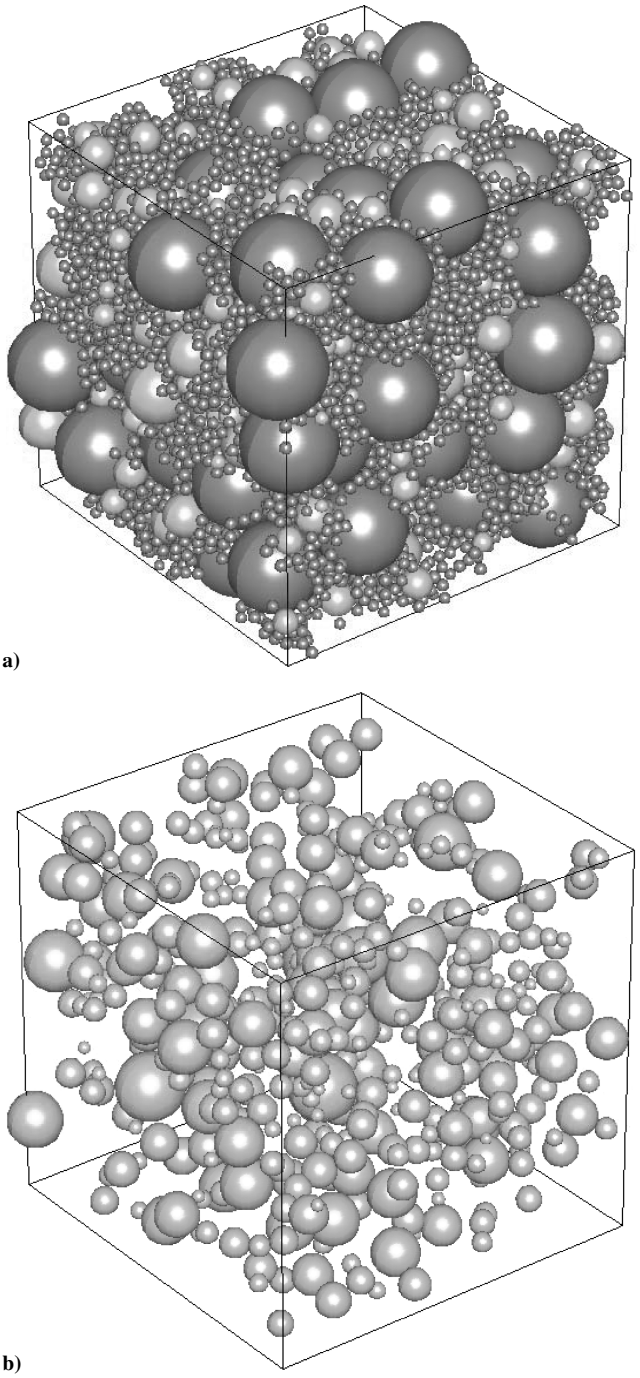

**Fig. 1 A 10,000-particle pack. a) AP (gray) and aluminum (copper) particles are shown. b) The AP spheres have been removed to better visualize the aluminum distribution. The pack consists of 18% by weight 45-$\mu$m-diam aluminum, 56.8% by weight 137.5-$\mu$m-diam (coarse) AP, 14.2% by weight 17.5-$\mu$m-diam (fine) AP, and 11% by weight binder. A log-normal distribution is used for the aluminum.**

A final issue to be discussed in this Introduction is the definition of the agglomeration fraction and uncertainties in this connection in the experimental literature. The key difficulty is that real propellants have a distribution of aluminum sizes, and it is not apparent how one can distinguish an original single particle from an agglomerate of comparable size. For example, if the initial distribution of a 23-$\mu$m cut ranges from 5 to 100 $\mu$m, then any final particle smaller than 100 $\mu$m and bigger than 6.3 $\mu$m (the size of two agglomerated 5-$\mu$m particles) could be an original or it could be an agglomerate.

The agglomeration fraction $f_{\text{agglom}}$ can be formally defined as the fraction of initial particles that form agglomerates $N_{\text{agglom}}/N$. The agglomerated weight fraction is then

$$\frac{\sum_{\text{agglom}} D_i^3}{\sum D_i^3} \tag{4}$$

where the numerator is a sum over agglomerates and the denominator is a sum over all particles. And the weight-mean diameter of the agglomerates is

$$D_{\text{aggl}} = \frac{\sum_{\text{agglom}} D_i^4}{\sum D_i^3} \tag{5}$$

However, as we have noted, an experimentalist cannot provide this information.

An alternative definition introduces the parameter $\langle \text{cut} \rangle$, where it is assumed that any final particle with a diameter greater than or equal to $\langle \text{cut} \rangle$ is an agglomerate, and any with a diameter smaller than $\langle \text{cut} \rangle$ is an unagglomerated particle. Note that insofar as the effects of aluminum are concerned, whether a particle is an agglomerate or not is of no consequence. But we need some way of testing theoretical predictions of the final particle distribution with experiment, and using $\langle \text{cut} \rangle$ makes that possible. Then if we start with $N$ particles and after the agglomeration process $N_p$ particles have diameters smaller than $\langle \text{cut} \rangle$, the pseudoagglomeration fraction is

$$f_{\langle \text{cut} \rangle} = (N - N_p)/N \tag{6}$$

The final number of particles is of course smaller than $N$ unless there has been no agglomeration. Equation (4) is still valid where now the sums over agglomerates are sums over particles with diameters greater than or equal to $\langle \text{cut} \rangle$. And the weight-mean diameter [compare Eq. (5)] is now given by the formula

$$D_{\langle \text{cut} \rangle} = \frac{\sum_{\langle \text{cut} \rangle} D_i^4}{\sum D_i^3} \tag{7}$$

This strategy is used in Ref. 10 with a choice $\langle \text{cut} \rangle = 49\,\mu\text{m}$.

A closely related issue in that it affects what is being measured is the location of the agglomerate collection point. Not all of the experimental reports are specific in this connection. But if the point is not sufficiently close to the surface, burn-up will have commenced, and some of the aluminum will have been converted to aluminum oxide smoke and lost from the particles.

The structure of the paper is as follows. In Sec. II we describe agglomeration models defined by proximity criteria. The simplest, model A, assumes that the proximity or agglomeration domain is spherical, characterized by a single parameter, the sphere radius. Model B, which comes in two flavors, assumes that the proximity domain is cylindrical, and this is characterized by two parameters, the radius and the height.

In Sec. III we examine experimental data and use these data to determine the parameters of one or more of the agglomeration models. Section III.A examines the propellant SME 8061 and fits the spherical radius of model A to match the number-median agglomerate diameter. The predicted distribution is then compared with the experimental distribution. Corrections as a result of combustion between the propellant surface and the agglomerate collection point are examined in Sec. III.B. Section III.C examines the propellant SME 90418 and fits the spherical radius of model A to match the number-median agglomerate diameter at different pressures. In addition, because the experimental data determine the height of the cylinder of model B, its radius can be chosen to fit the mean agglomerate diameter, and this permits a meaningful comparison between the distribution predicted by model A and those predicted by the two variations of model B. Section III.D examines the propellant used in the space shuttle boosters. Here also we are able to compare the predicted and measured distributions once the mean agglomerate diameter has been matched. And in Sec. III.E propellant data reported by Sambamurthi et al. are examined.[10] These data afford no validation, but enable us to examine how the proximity sphere radius varies with pressure and with the size of the fine AP in a bimodal AP distribution.

Section IV describes multiphase rocket-chamber flow simulations including fluid transport, aluminum drop transport, and smoke transport. Propellant surface agglomerate data are used to define the boundary conditions associated with aluminum injection into the chamber. The key result is a prediction of the aluminum distribution at the nozzle.

## II. Agglomeration Models

In this section we describe three agglomeration models rooted in a random packing formulation. Model A is characterized by a spherical agglomeration domain. Models B1 and B2 are characterized by a cylindrical domain and differ only in that B2 incorporates a melting criterion, B1 does not.

### A. Model A

The first model is an isotropic one: it accounts only for proximity, and so is characterized by but a single parameter. Not that we are suggesting that agglomeration can be characterized by a single parameter; the random packs that we use contain, implicitly, all of the parameters of formulas (1) and (2) (and more). And so the agglomeration model includes all of these plus a lumping parameter (the critical proximity radius) that is controlled by surface residency, surface mobility, burning rates, etc. There is no a priori expectation that a model as simple as this can do the job, but our strategy is rooted in the philosophy that one starts with the simplest conceivable model and only adds complexity should it prove deficient.

Moreover, there is another way of looking at this strategy. On its face, it is an attempt to predict agglomeration details by making use of the pack morphology and a single empirical constant. But it can also be seen as the answer to the following question: Given experimental agglomeration data, how close were the original particles that formed these agglomerates? Later one can then ask whether the answer to this question can be related to the underlying physics.

For any two aluminum spheres $(i, j)$ with radii $r_i, r_j$ and centers located at $(x_i, y_i, z_i)$, $(x_j, y_j, z_j)$, we define a separation distance $S_{i,j}$ by

$$S_{i,j} = \sqrt{(x_i - x_j)^2 + (y_i - y_j)^2 + (z_i - z_j)^2} - r_i - r_j \tag{8}$$

If $S_{i,j}$ is less than a critical separation distance $S_d$, the two spheres will agglomerate.

The algorithm proceeds as follows:

1) Given an initial propellant formulation (size and size distribution of AP and aluminum), construct a three-dimensional pack of spheres that has the same packing fraction as the experimental data set; typically, the packing fraction is between 86 and 88% by weight of total solids. Although various packing algorithms can be used, we use the dynamic packing algorithm developed in house and described fully in Refs. 8 and 9. The output includes a random distribution of aluminum spheres with centers $(x_i, y_i, z_i)$ and radii $r_i$. Figure 1 shows a typical output.

2) Postprocess the pack by ordering the aluminum particles from top to bottom using the $z$ coordinate. A table of $N$ entries is generated, where $N$ is the total number of aluminum particles, whose $z$ coordinate is in descending order.

3) Choose a value for the separation distance $S_d$.

4) Initially tag each particle with a flag $tag(i) = 0$, and set the agglomeration counter to zero ($aggl_{\text{num}} = 0$). The agglomeration counter is the total number of agglomerates.

5) Set $i = 1$.

6) In the table, search for all particles $j > i$ whose distance $S_{i,j}$ is less than $S_d$. There are three cases to consider when $S_{i,j} < S_d$:

(a) If $tag(i) = 0$ and $tag(j) = 0$, increment $aggl_{\text{num}}$ by 1 and set $tag(i) = tag(j) = aggl_{\text{num}}$. This marks the beginning of a new agglomerate.

(b) If $tag(i) \neq 0$ and $tag(j) = 0$, set $tag(j) = tag(i)$.

(c) If $tag(i) = 0$ and $tag(j) \neq 0$, set $tag(i) = tag(j)$.

Note that separate branches of the tree are not allowed to agglomerate [i.e., there are no consequences if $tag(i) \neq 0$ and $tag(j) \neq 0$.] This prevents the possibility of creating a superagglomerate formed by a single chain of aluminum particles encompassing a coarse AP particle.

7) Increment $i$ by 1; if $i < N$, go to step 6.

8) Group all particles with the same $tag$ number. These constitute the agglomerates. All particles with $tag = 0$ leave the surface unagglomerated.

9) Compute the agglomeration fraction; if the computed agglomeration fraction is equal to the experimental value, stop. If not, choose a new value of $S_d$, and go to step 3. Thus the agglomeration fraction is always matched, but the distribution, mean diameter, etc., are predicted. We can also carry out an iteration to capture the mean diameter, and then the agglomeration fraction is predicted.

Consider the example shown in Fig. 2. For $i = 1$, $S_{1,3}$ is found to be less than $S_d$ (say), while $S_{1,2}$, $S_{1,4}$, $S_{1,5}$, $S_{1,6}$, and $S_{1,7}$ are greater than $S_d$. Set $tag(1) = tag(3) = 1$; these two particles will now constitute agglomerate number one. For $i = 2$, $S_{2,3}$ is less than $S_d$. Because $tag(2) = 0$ and $tag(3) = 1$, set $tag(2) = tag(3)$. Particle 2 is now part of agglomerate number 1. $S_{2,5}$ is less than $S_d$; set $tag(5) = tag(2)$. $S_{2,4}$, $S_{2,6}$, and $S_{2,7}$ are greater than $S_d$. Particles 1, 2, 3, and 5 now form a single agglomerate. Continue incrementing $i$, and we see that particles 4 and 6 form agglomerate number 2, whereas particle 7 leaves the surface unagglomerated.

We now apply the algorithm of model A to the sample propellant shown in Fig. 1. The value of $S_d$ is chosen to be 5 $\mu$m. Five groups of particles (color coordinated) that form separate agglomerates are shown in each panel of Fig. 3.

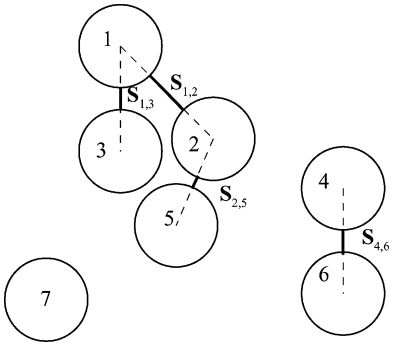


**Fig. 2 Sketch of seven aluminum particles, with some of the distances $S_{i,j}$ labeled.**

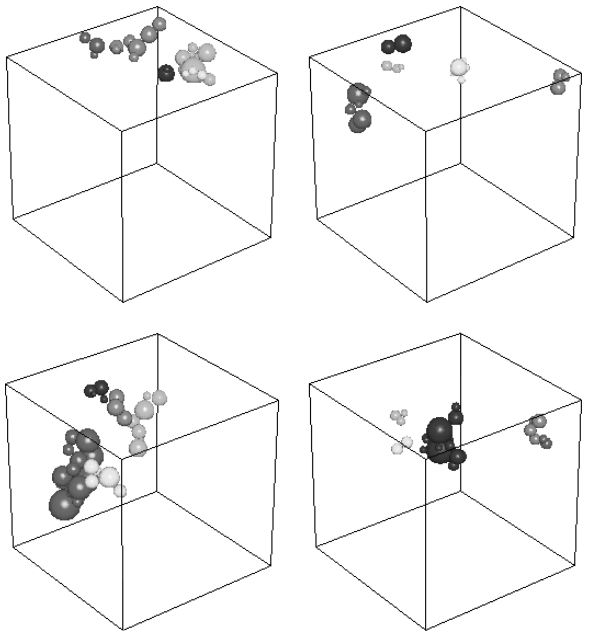

**Fig. 3 In each panel, five groups of aluminum spheres that form separate agglomerates are shown (color coordinated). The original pack is shown in Fig. 1. The separation distance used to generate this figure is $S_d = 5$ $\mu$m using agglomeration model A.**

### B. Model B

The second agglomeration model takes into account the mean surface residence time and the observation that aluminum particles can move over the propellant surface because of the presence of binder melt layers and surface tension gradients. Detachment—the end of residence—is not well understood, but occurs when vertical aerodynamic forces overcome vertical surface-tension forces.

To model the effect of the mean residence time on the agglomeration process, we define the distance $d_{i,j}\,(i < j)$ to be the vertical distance between the bottom of particle $i$ and the top of particle $j$; see Fig. 4. Thus,

$$d_{i,j} = (z_i - r_i) - (z_j + r_j) \tag{9}$$

Define $S_1 = r_b\tau$ to be the distance the surface travels downward in the normal direction in time $\tau$, where $r_b$ is the mean burn rate and $\tau$ the mean residence time. Agglomeration is only possible if

$$d_{i,j} \leq S_1 \tag{10}$$

To model the movement of an aluminum particle along the surface, we define the distance

$$g_{i,j} = \sqrt{(x_i - x_j)^2 + (y_i - y_j)^2} - r_j \tag{11}$$

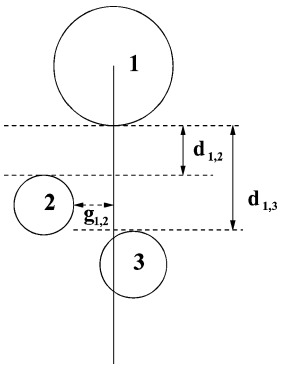


**Fig. 4 Sketch of three aluminum particles for model B.**

(see Fig. 4). In this figure $g_{1,2}$ is a positive number, while $g_{1,3}$ is negative as particle 3 is cut by a vertical line through the center of particle 1. Let $G_{i,j} = \max(0, g_{i,j})$. Agglomeration is only possible if

$$G_{i,j} \leq S_2 \tag{12}$$

where $S_2$ must be defined for each propellant. In general it will be a function of pressure and propellant composition.

Agglomeration takes place only when both criteria are satisfied, that is, when

$$d_{i,j} \leq S_1 \qquad \text{and} \qquad G_{i,j} \leq S_2 \tag{13}$$

Except for obvious modifications, the algorithm presented for model A remains unchanged.

*Remark:* This model requires the mean residence time and an estimate of mobility along the surface.

*Remark:* The mean residence time $\tau$ can be defined as a random variable with some distribution about a mean. And the distance $S_2$ can be defined in terms of a random walk.

*Remark:* Cohen's melting criteria for aluminum[7] can be incorporated into this model as a constraint [Eq. (3)]. For the data of Table 1, variations with $r_b$ of the critical melting diameter $D_{\text{melt}}$ are shown in Fig. 5. We call the case without the melting constraint model B1, and the case with the melting constraint model B2. Note that Eq. (3) (and therefore Fig. 5) is generated by a crude analysis and has not been verified using simulations.

**Table 1 Parameter values used for Cohen's melting criteria (The surface temperature is described by a linear function of the burn rate.)**

| Parameter | Value |
|---|---|
| $\lambda_B$ | $6.59 \times 10^{-4}$ cal/(cm s K) |
| $\rho_B$ | 0.92 g/cm$^3$ |
| $\rho_{\mathrm{Al}}$ | 2.70 g/cm$^3$ |
| $c_B$ | 0.67 cal/(g K) |
| $c_{\mathrm{Al}}$ | 0.21 cal/(g K) |
| $T_m$ | 933.0 K |
| $T_0$ | 300.0 K |
| $T_s$ | $1100 - (1 - r_b) * 142$ K |

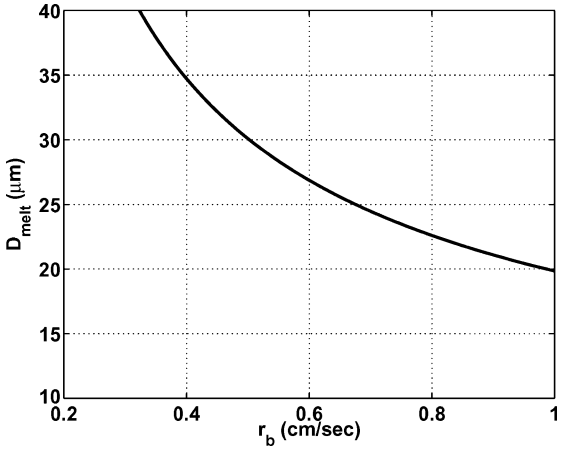


**Fig. 5 Plot of the critical melting diameter $D_{\mathrm{melt}}$ as a function of burn rate $r_b$, deduced from Cohen's formula [Eq. (3)] and the data of Table 1.**

## III. Agglomeration Size and Size Distribution

In this section results for the agglomerate size and size distributions are obtained for four propellant formulations: SME (SNPE Matériaux Energétiques, France) Propellant 8061, SME Propellant 904118, the space shuttle booster propellant, and a propellant used in Ref. 10. Each data set is calibrated separately, and in the case of 904118 we compare the results generated by all three models, A, B1, and B2.

### A. SME Propellant 8061 Data

Our first example is SME Propellant 8061 (Ref. 11). We examine this because the agglomerate distribution is given, and this provides an important validation test of our strategy. The propellant consists of 18% by weight 45-$\mu$m aluminum, 68% by weight AP, and 12% by weight binder. The AP is bimodal with a mean diameter of 13.2 $\mu$m for the fine, 241 $\mu$m for the coarse, and we have chosen a log-normal distribution for these modes. The initial aluminum distribution is in the range [7.7 $\mu$m, 112.1 $\mu$m] with mean 45 $\mu$m and is shown in Fig. 6. In Fig. 7 we compare the results of model A for $S_d = 15$ $\mu$m with the experimental results. $S_d$ is chosen so that the theoretical number-median diameter matches the experimental value of 48 $\mu$m. The distribution (which includes all particles, agglomerated or not) agrees quite well for particles of diameter greater than the number median and very well for those larger than 100 $\mu$m, particles that are necessarily agglomerates (compare Fig. 6). The agreement for particles smaller than 48 $\mu$m is not good, but it is clear from the large number of experimental particles with diameters smaller than any of the initial particles that significant combustion has occurred, and our calculations do not account for this. It is something that will affect the small particles more than it will affect the large particles.

However, it is the large particles that are of practical concern, for in them resides most of the mass. And 90% of the mass resides in the particles in the last 25% of the cumulative number fraction, and 98% resides in the particles in the last 50% of the cumulative number fraction. Put simply, the model reasonably predicts the distribution of 98% of the mass of aluminum leaving the surface.

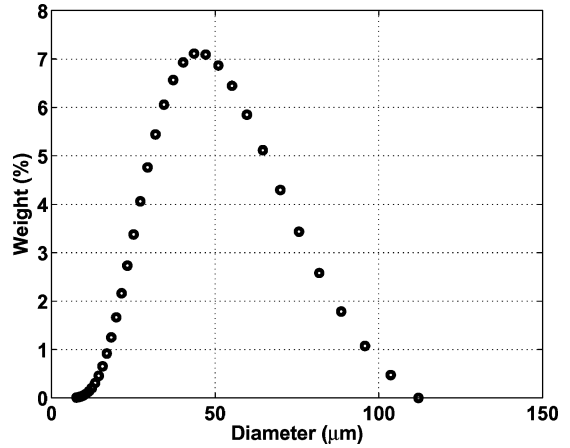


**Fig. 6 Plot of the initial aluminum distribution for SME Propellant 8061. This is a scatter plot for which only the data points have meaning, and the sum of the ordinates equals 100.**

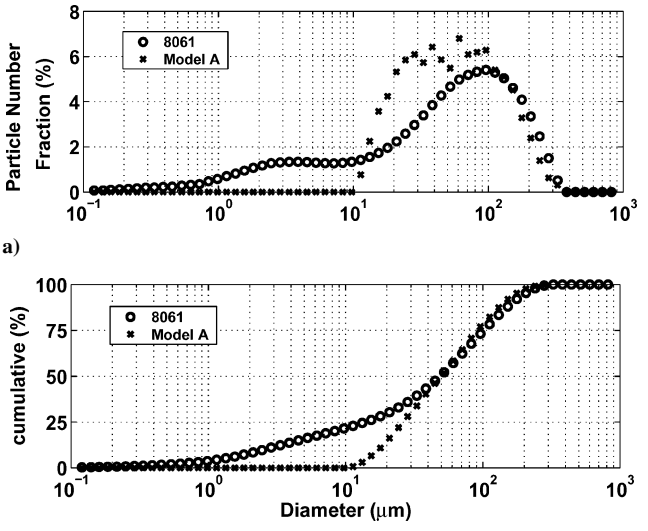


**Fig. 7 Comparison of SME Propellant 8061 data[11] and the agglomeration model A. This is a histogram, and the data are plotted at the midpoints of the bins, with the same bins used for both theory and experiment.**

That the single-parameter model can give results of this quality is, we believe, strong evidence that a modeling strategy primarily rooted in the propellant morphology predicted by the packing algorithm could be of significant value. We note that none of the existing models or curve fits discuss agglomeration distribution, and yet this is precisely what is needed by the rocket designer. Trubert's data are, for our purposes, by far the best that we have been able to find, characterized as they are by a richness of quantitative information.

### B. Propellant 8061, Accounting for Combustion

It is not our purpose in this paper to examine the near-surface behavior of the agglomerates after they leave the surface. (The calculations of Sec. IV are on the much larger scale of the rocket chamber.) Nevertheless, the quality of Trubert's data[11] has tempted us to estimate, in as simple a fashion as possible, how the distribution of Fig. 7a could be modified if combustion is accounted for between the surface and the collection point 5 mm above the surface. To this end, we use the following model, one that allows for burning, but not for oxide accumulation on the agglomerate.

The particle dynamics is described by the equations

$$M_p \frac{\mathrm{d}v_p}{\mathrm{d}t} = F, \qquad \frac{\mathrm{d}x_p}{\mathrm{d}t} = v_p \tag{14}$$

where $M_p = \rho_p \pi D^3/6$ is the particle mass, $F$ is the force acting on it, $D$ is the particle diameter, and $x_p$, $v_p$ are its location and velocity. The force is given by the formula

$$F = \text{signum}(v_g - v_p)\rho_g (v_g - v_p)^2 \pi D^2 c_D/8 \tag{15}$$

where $\rho_g$ is the gas density, $v_g$ its velocity, and $c_D$ is the drag coefficient. Then $c_D$ is given by the formula for a sphere:

$$c_D = \begin{cases} 24/Re & Re \le 0.34 \\ 0.48 + 28\, Re^{-0.85} & Re > 0.34 \end{cases} \tag{16}$$

where

$$Re = |v_g - v_p|\rho_g D/\mu_g \tag{17}$$

$\mu_g$ being the gas viscosity.

The particle diameter changes according to Hermsen's formula[12]

$$D = D_0 \left(1 - \frac{kt}{D_0^{1.8}}\right)^{1/1.8} \tag{18}$$

where

$$k = 8.3314 \times 10^{-5} R_k\, a_k^{0.9}\, P^{0.27} \text{cm}^{1.8}/\text{s} \tag{19}$$

when $P$, the pressure, has dimensions of pounds per square inch. Note that the familiar $D^2$ law of drop burning follows from elementary dimensional considerations if there is only a single length scale (the drop diameter) so that the $D^{1.8}$ law identified here implies the existence of at least two length scales.

With $S_d$ assigned, the agglomeration strategy yields the distribution at the surface, and then these equations are integrated out to $x_p = 5$ mm to determine the modified distribution. $S_d$ is taken to be 22 $\mu$m rather than the value 15 $\mu$m used in the absence of combustion; other parameter values are listed in Table 2. None of them (apart from $S_d$, as always) have been chosen to optimize the fit with Trubert's experimental data.

**Table 2 Parameter values for the calculations of Sec. III.B[a]**

| Parameter | Value |
|---|---|
| $P$ | 5 MPa |
| $r_b$ | 0.8 cm/s |
| $R_u$ | 1.9859 kcal/kmol K |
| $MW$ | 28.34 kg/kmol |
| $T_g$ | 3000 K |
| $\mu_g$ | $1.935 \times 10^{-3}$ g/cm-s |
| $\rho_g$ | $(PMW)/(R_g T_g)$ g/cm$^3$ |
| $v_g$ | $r_b\, V_{\text{blend}} \rho_{\text{blend}}/(V_g \rho_g)$ cm/s |
| $R_k$ | 2.7 |
| $a_k$[b] | 17 |
| $\rho_p$ | $(5632 - 1.127 T_g) \times 10^{-4}$ g/cm$^3$ |
| $m_s$[c] | 0.18 |
| $m_{\text{Ap}}$[c] | 0.68 |
| $m_b$[c] | 0.14 |
| $\rho_s$ | 2.70 g/cm$^3$ |
| $\rho_l$ | 2.35 g/cm$^3$ |
| $\rho_{\text{Ap}}$ | 1.95 g/cm$^3$ |
| $\rho_b$ | 0.92 g/cm$^3$ |
| $V_l$ | $V_s \rho_s/\rho_l$ |
| $V_g$ | $1 - V_l$ |

[a]The solid phase comprises aluminum, AP, and binder; the fluid phase comprises gas and liquid aluminum, which has a lower density than that of solid aluminum: $m$ are mass fractions, $V$ are volume fractions; the subscripts are $s$—aluminum solid phase, $l$—aluminum liquid phase, Ap—AP, $b$—binder, $g$—gas phase; blend—combined AP and binder (excluding the aluminum). Many of the values come from Ref. 13.
[b]$a_k$–average reported in Ref. 14.
[c]The pressure, burn rate and mass fractions $m_s$, $m_{\text{Ap}}$, $m_b$ are reported in Trubert.[11]

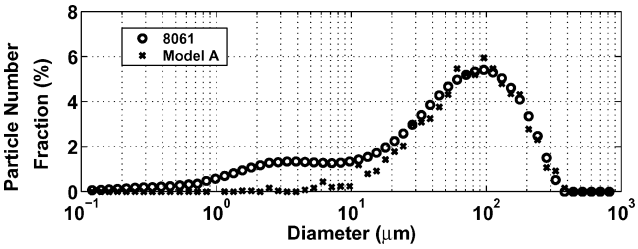


**Fig. 8 Distribution calculated for propellant 8061 when partial agglomerate burning is accounted for (compare Fig. 7).**

An obvious flaw in this strategy is that the burning law, Eq. (18), is only valid on the upper branch of the burning response in the burning-rate/Damköhler-number plane, where, in classical theory, the solution beyond the reaction zone or flame sheet differs little from the Burke–Schumann solution. At sufficiently small Damköhler numbers (small drop sizes) the solution necessarily lies on a lower branch where a formula different from Eq. (18) is necessary. The burning rate on this lower branch will be much lower. And so, in our calculations we stop the burning of a particle when its diameter falls below 1 $\mu$m, an arbitrary choice. Thus the particle is kept and contributes to the final number fraction.

The modified distribution, calculated in this way, is shown in Fig. 8. Essentially we have no particles of diameter less than 10 $\mu$m except for the 26% at 1 $\mu$m (off scale). These represent the distribution observed by Trubert below 10 $\mu$m, a distribution that our simple model can not capture, a distribution that undoubtedly includes smoke. Clearly our results for diameters greater than 10 $\mu$m would not be affected if we chose a burning cutoff at any diameter smaller than 10 $\mu$m.

An equivalent comparison between the experimental data and theory for diameters greater than 10 $\mu$m could be generated by choosing $\langle \text{cut} \rangle = 10\,\mu$m, and then the sum in the bins to the right of 10 $\mu$m would be 100, rather than 74, as here.

The agreement between theory and experiment for diameters greater than 10 $\mu$m is surprisingly good, and this might well be happenstance. But a comparison of Fig. 8 with Fig. 7 gives a good indication of how combustion can signficantly affect experimental agglomeration data.

A final note on this propellant. The initial number of aluminum particles that were examined equals 67,684. The number of agglomerates/particles defined by the choice $S_d = 15$ equals 4810. The number of agglomerates/particles defined by the choice $S_d = 22$ equals 2525 before burning, and after burning 1857 of these have diameters greater than 10 $\mu$m. And when we do not use a proper distribution for the aluminum, but assume that it consists only of particles of diameter 45 $\mu$m, the predictions bear little relationship to the experimental data. A large peak, in the neighborhood of 30%, is found in the 45–50 $\mu$m range, and the distribution of particles greater than 100 $\mu$m is in error by an order of magnitude.

### C. SME Propellant 904118 Data

Our next example is SME Propellant 904118 (Ref. 15). We examine this because the experimental data define $S_1$, leaving but a single parameter $S_2$ to be chosen, and so it is of interest to compare the predictions of model A with those of models B1 and B2. The propellant consists of 18% by weight 30-$\mu$m aluminum, 68% by weight AP, and 12% by weight binder. The AP is bimodal with a mean diameter of 10 $\mu$m for the fine and a mean diameter of 200 $\mu$m for the coarse. Figure 9 plots the agglomeration diameter (here defined as the number median, with $\langle \text{cut} \rangle = 80\,\mu$m) against the pressure and the inverse of the burn rate (see Table 3). The dashed lines are least-squares fits.

We now compare the results from model A with the experimental results. Because the size distribution for the AP particles is not given, we take for each of the two modes a single size, and this introduces unavoidable uncertainties into our predictions. The initial aluminum distribution (Fig. 10) is taken to be a log-normal distribution with

**Table 3 Values of the pressure, burning rate, agglomerate mean diameter, and mean residence time for SME Propellant 904118 reported in Ref. 15**

| Pressure, MPa | Burning rate, cm/s | Diameter, $\mu$m | Residence time, ms |
|---|---|---|---|
| 4.0 | 0.7 | 125 | 2.4 |
| 3.0 | 0.635 | 138 | 2.81 |
| 1.5 | 0.5 | 150 | 3.54 |
| 0.2 | 0.27 | 170 | 4.6 |

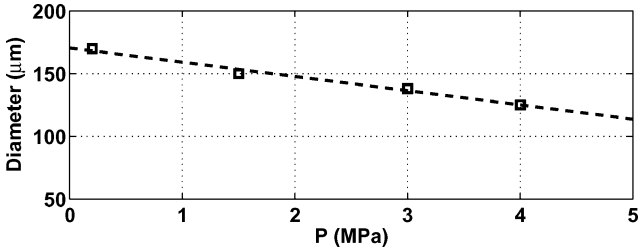


a)

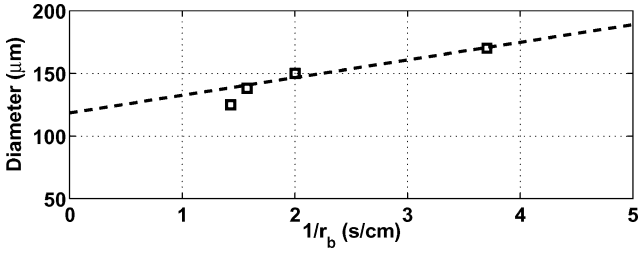


b)

**Fig. 9 Plot of the agglomeration diameter from Ref. 15 against a) pressure and b) inverse of the burn rate for SME Propellant 904118. The lines are least-squares fits.**

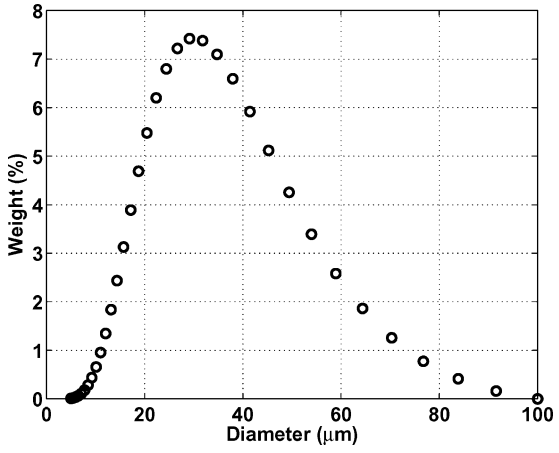


**Fig. 10 Plot of the initial aluminum distribution for SME Propellant 904118. This is a scatter plot, as in Fig. 6.**

mean 30 $\mu$m over the range [5 $\mu$m, 100 $\mu$m], numbers provided by Duterque,[15] but our assumption as to the form of the distribution, yet another uncertainty. We choose $S_d$ at each pressure so that the mean agglomerate diameter (with a cutoff diameter of 80 $\mu$m) matches the experimental data in Fig. 9; the results are shown in Fig. 11. The corresponding distributions for the two pressures 1.5 and 4.0 MPa are shown in Fig. 12, along with logarithmic fits. Note that for the lower pressure the distribution is broader than it is for the higher pressure, a well-known characteristic of the experimental record, and one that is easy to understand. For example, the surface residence time increases with decreasing pressure, Table 3, so that the size of the agglomeration domain increases. It is of value that

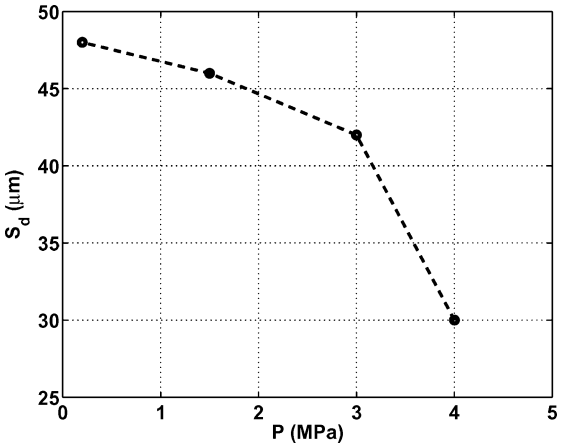


**Fig. 11 $S_d$ at different pressures to match the number-median agglomeration diameter for propellant 904118.**

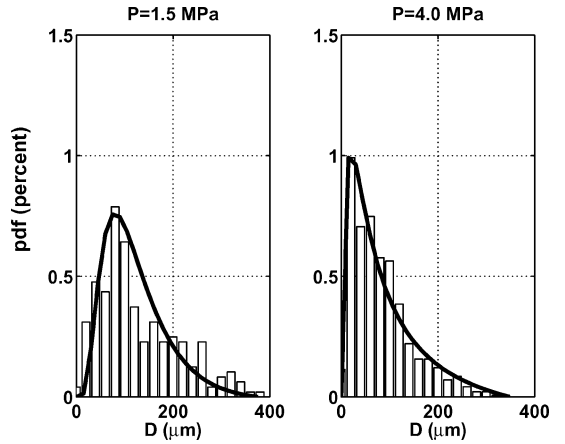


**Fig. 12 Distributions for propellant 904118 at two pressures, predicted by model A. These are PDFs, so that the area defined by the bins and by the curve fits (logarithmic) = 100.**

our model yields such information because large-scale solid-rocket-motor simulations require both particle size and size distribution, and the manner in which these vary with pressure as the latter varies in both time and position in the chamber.

The data of Table 3, including as it does both the burning rate and the surface residence time (and therefore $S_1$), enable us to use models B1 and B2 with but a single parameter at our disposal, $S_2$. Thus at $P = 4$ MPa, we have $S_1 = 16.8\,\mu$m. Then with $S_2$ chosen so that the mean diameter of the agglomerates is 125 $\mu$m (compare Table 3), we have $S_2 = 40\,\mu$m for model B1, 75 $\mu$m for model B2. The corresponding distributions are shown in Fig. 13, together with that predicted by model A. The agreement between A and B1 is excellent, suggesting that despite the different physical roots of $S_1$ and $S_2$ combining them into the single proximity parameter of model A could work well. However, horizontal migration of the largest particles in the melt layer might be hampered by the AP and, if this were properly accounted for, generate differences between the predictions of A and B1. The distribution defined by B2 differs significantly, but contains an ingredient absent in A and B1, namely, the melting criterion. We have no reason to believe that the latter is accurate, and evidence that it is not. For two-dimensional configurations, the code described in Refs. 3 and 4 can be used to calculate the temperature rise of an aluminum disk during its passage through the propellant, which can be compared to the two-dimensional version of Eq. (3). We have done that, and agreement is poor. We hope to make similar comparisons in three dimensions, but technical difficulties force us to defer these calculations.

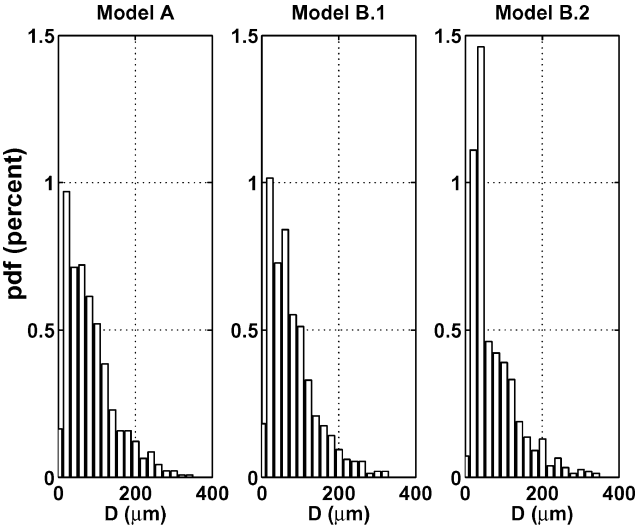


**Fig. 13 Predicted distributions for propellant 904118 (compare Fig. 11).**

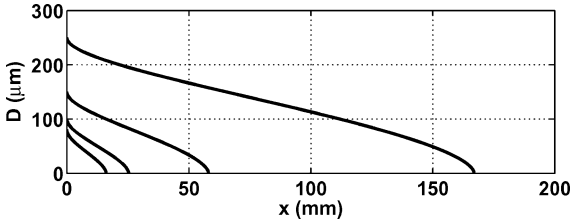


**Fig. 14 Estimated particle history for the motor of Ref. 16 (shuttle propellant) using the model of Ref. 12. $x$ is the distance from the propellant surface.**

### D. Shuttle Data

Our next example is the space shuttle propellant data given in Ref. 16. We examine this partly because there is particular interest by the Center for Simulation of Advanced Rockets[§] in the space shuttle boosters.

The propellant consists of 16% by weight of 23-$\mu$m aluminum, 48.8% by weight of 200-$\mu$m AP, 20.9% by weight of 30-$\mu$m AP, and 14% by weight of binder. Because the size distributions for the two AP cuts are not given, we take single sizes. For the aluminum we take a log-normal distribution with mean 23 $\mu$m and a range [7.5 $\mu$m, 84 $\mu$m], although only the range is specified by Laredo et al.[16] So here, as in the preceding section, lack of knowledge of both the AP and the aluminum distributions introduces uncertainties. Moreover, the agglomerates are collected 2 cm from the propellant surface (in a 25-cm-long rocket chamber), and rough estimates using the model of Hermsen[12] suggest significant burn-up of the smaller particles (of diameter less than 100 $\mu$m or so) at that distance, Fig. 14 (compare Sec. III.B). Moreover, it is puzzling that the experimental data include no particles smaller than 90 $\mu$m. The pressure is $P = 3.6$ MPa, and $r_b = 8.8$ mm/s. The mean diameters are Sauter means (surface area preserving). With $\langle \text{cut} \rangle = 85$ $\mu$m, and using model A, $S_d$ is set equal to 23.1 $\mu$m so that the Sauter mean of the agglomerates matches the experimental value of 132 $\mu$m. The distribution that we then obtain is shown in Fig. 15, where it is compared to the experimental distribution. The agreement is unsatisfactory. Figure 16 shows the distribution that we get if all particles are retained. The differences here are easily accounted for by the uncertainties in the data and the unaccounted-for combustion, and this highlights the fact that when agglomeration data are obtained without the needs of the modeler in mind (a quite understandable situation) it can have limited value for validation.

It is of some interest that the value of $S_d$ identified here is comparable to the values identified in the earlier sections, which one might expect. If $S_d$ is fitted using a definition of the mean different from that of the experimental data (and we know this because we made this error in early calculations), variations of $S_d$ between one propellant and another can be unreasonably large.

[§]Information available online at http://www.csar.uiuc.edu.

**Table 4 Size and size distribution of propellant ingredients (from Sambamurthi et al.[10])**

| Ingredient | Nominal size, $\mu$m | Size range, $\mu$m |
|---|---|---|
| AP | 390 | 355–425 |
| AP | 196.0 | 180–212 |
| AP | 82.5 | 75–90 |
| AP | 49.0 | 45–53 |
| AP | 17.5 | 0–37 |
| Al | 30.0 | 10–80 |

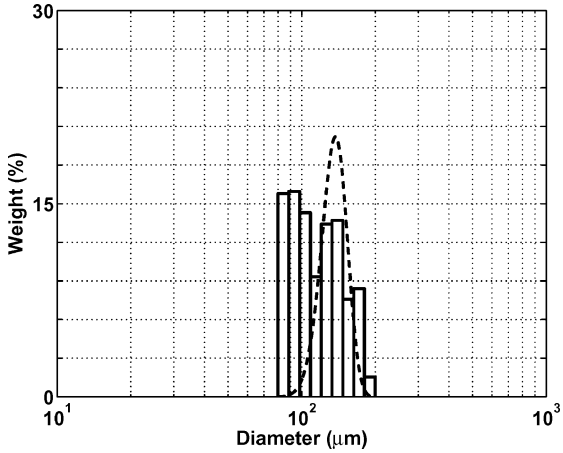


**Fig. 15 Distributions for the shuttle propellant. The – – – curve is the boundary of the experimental histogram[16]; the histogram is the theoretical prediction.**

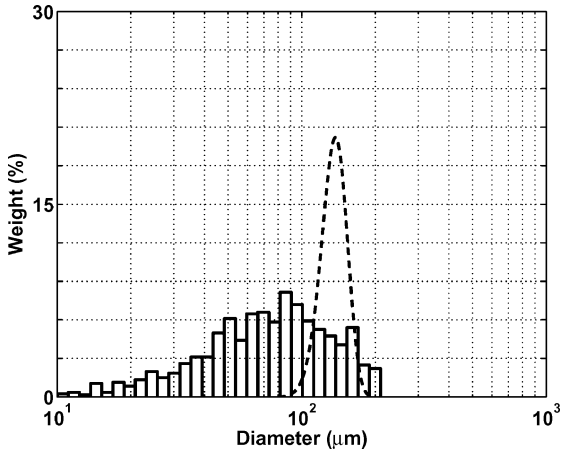


**Fig. 16 Redrawing of Fig. 15 (shuttle propellant) keeping all of the particles in the theoretical histogram.**

### E. Data of Sambamurthi, Price, and Sigman

An extensive agglomeration data set is given in Ref. 10. Unfortunately, only the mean agglomerate diameter $D_{\langle 49 \rangle}$ is given, and because we can always choose $S_d$ to match any diameter we cannot use these data for validation. Nevertheless, we carry out calculations so that the variations of $S_d$ with pressure and with the size of the fine AP in the bimodal mix can be described. We use a subset of the data.

The AP and aluminum size and size distribution are shown in Table 4. For each propellant formulation the AP is taken to be

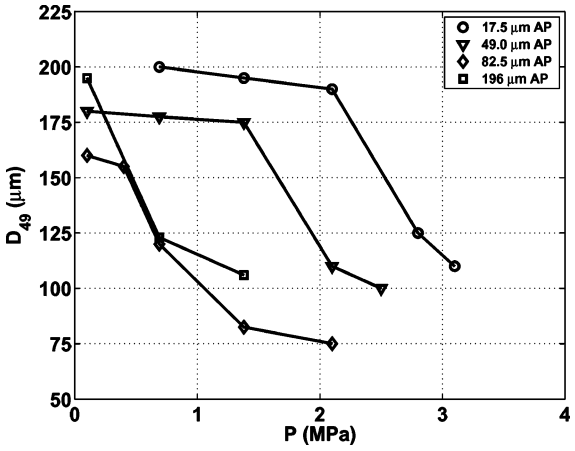


**Fig. 17 Plot of the agglomeration diameter $D_{\langle 49\rangle}$ as a function of pressure for various fine AP sizes; adapted from Sambamurthi et al.[10]**

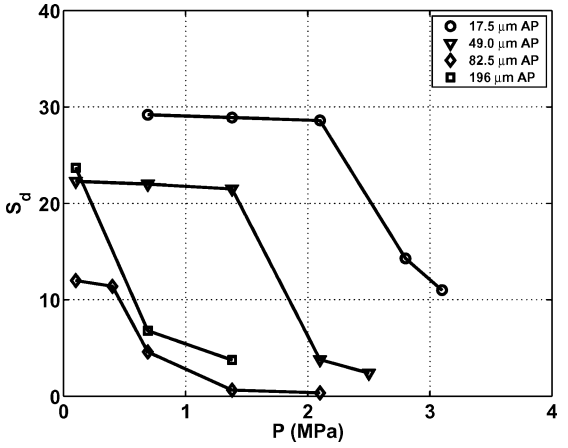


**Fig. 18 Plot of the separation distance $S_d$ as a function of pressure for various fine AP sizes, chosen to fit the data of Fig. 16 (propellant of Sambamurthi et al.[10]).**

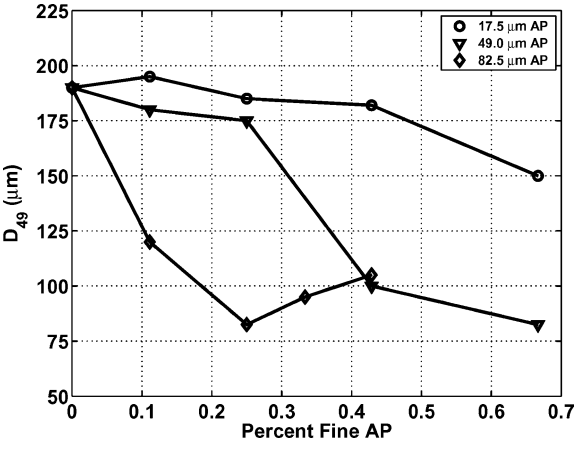


**Fig. 19 Plot of the agglomeration diameter $D_{\langle 49\rangle}$ as a function of $R$ for various fine AP sizes; adapted from Sambamurthi et al.[10]**

bimodal with the coarse size fixed at 390 $\mu$m and the fine size varied. The volume ratio of fine AP to coarse AP is $R$, a variable.

Figure 17 is a plot of the agglomerate diameter $D_{\langle 49\rangle}$ vs pressure for four AP fine sizes and $R$ fixed at the value 0.8. Figure 18 shows the choices of $S_d$ needed to match these diameters, and it is clear that these values can get quite small when $D_{\langle 49\rangle}$ is small and the fine AP size is large. This is to be expected. Figures 19 and 20 show similar results when $R$ is varied and the pressure is fixed at 1.38 MPa.

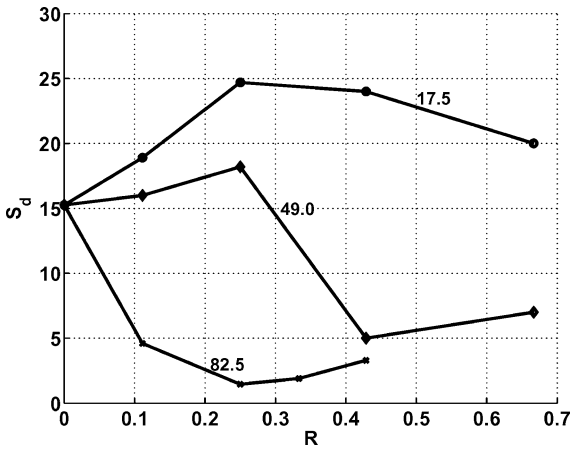


**Fig. 20 Plot of the separation distance $S_d$ as a function of $R$ for various fine AP sizes. Chosen to fit the data of Fig. 18 (propellant of Sambamurthi et al.[10]).**

## IV. Multiphase Flow Simulations in Rocket Motor

So far in this paper we have only discussed the aluminum distribution at the propellant surface. As the aluminum burns and passes through the chamber, this distribution is changed significantly, and it is of considerable interest to predict the distribution at the nozzle because that plays a key role in defining slag accumulation in reentry nozzles, nozzle erosion, and exhaust signatures. Here we present some sample calculations, partly to demonstrate some of the tools that are now available at the Center for Simulation of Advanced Rockets[¶] and partly to give concrete examples of the kinds of changes that occur between the propellant surface and the nozzle and the kinds of distributions that can occur at the nozzle.

To assess the effects of the aluminum distribution synthesized from the agglomeration models, we have performed computational-fluid-dynamics simulations in a representative rocket motor. To this end, a multiphysics integrated computational framework consisting of an Eulerian all-speed gas solver, a Lagrangian particle-tracking module, an Eulerian oxidizer species module, and an equilibrium Eulerian module for the smoke (alumina) particles is used. The gas flow inside the chamber core is described by the time-dependent all-speed compressible Navier–Stokes equations, governing the evolution of mass, momentum, and energy. Because of the size of the aluminum droplets at the propellant surface, a Lagrangian formalism is adopted, where the evolution of the droplet positions, mass, momentum components, and energy is solved. The droplet burn rate is based on empirical correlations and is a complex function of gas temperature and pressure, droplet diameter, and effective oxidizer.[17] A scouring smoke process permits the aluminum droplet to scavenge smoke particles as they pass through a cloud of smaller smoke particles. Alumina are represented by a continuum concentration field whose evolution is given by an advection-diffusion equation. The smoke velocity is obtained from an equilibrium Eulerian approximation, where the smoke velocity is expressed in terms of the local gas velocity with a correction factor.[18] Various sources of mass, momentum, and energy exchanges arise and are formulated in a thorough manner through a module called Rocinteract. Further details are described in Ref. 19.

An important component in evolving the Lagrangian aluminum droplets in the rocket chamber is an appropriate description of the injection process at the propellant surface. In the past, several efforts in the literature have assumed the injection to be at a fixed rate in both time and distance. However, the actual injection process, as seen in experimental visualizations and measurements, is complex and occurs randomly in space and time. The injection module requires the following parameters to be specified at each time step: the number of droplets; their position coordinates on the injected

[¶]Information available online at http://www.csar.uiuc.edu.

surface; their initial mass, momentum components, and energy. We have developed a Markovian-based stochastic injection computational module that mimics the natural mechanism occurring on the propellant surface. The model encompasses several distributions including constant size, logarithmic normal, and skewed distributions. In the present study, distributions obtained from the agglomeration models of the random packs discussed in the preceding sections are synthesized and used as inputs to the injection model.

These physical models have been implemented numerically in a code suite, referred to as RocFluid. For unsteady simulations, all governing equations are integrated in time using a fourth-order-accurate Runge–Kutta scheme. Block-structure and unstructured finite volume based codes are used to evolve the gas flow. The suite of codes is parallelized and runs efficiently on a variety of parallel platforms with up to thousands of processors.[19]

To assess the effects of agglomeration-based injection parameters, a two-dimensional variation of the ONERA C1 configuration is used.[20] The model motor, shown in Fig. 21, has a length of 0.47 m and a half-height of 0.045 m. The propellant grain has a length 0.2 m, a thickness 0.015 m, and it tapers to zero thickness to create the main chamber. The location at which the propellant tapers results in the formation of a shear layer, leading to an instability and initiating a von Kármán vortex-shedding mechanism. We consider the full configuration without the use of a symmetry plane along the flow axis to allow for asymmetric disturbances. We also use a converging-diverging nozzle. The computational grid consists of $318 \times 61$ nonuniformly distributed cells in the $x$ and $y$ directions, respectively. The following properties for the gas mixture are used: $\gamma = 1.14$, $C_p = 2439.04$ J/(kgK), $\mu = 36.0 \times 10^{-5}$ kg/(ms), the injection temperature $T_{\text{inj}} = 3387$ K, and the injection mass rate $\dot{m}_g = 21.201$ kg/(m$^2$s). When two-dimensional single-phase (gas-only) simulations are performed, the results show an oscillation with a primary frequency of 2568 Hz, in good agreement with the secondary longitudinal mode of the chamber (2570 Hz).

The multiphase computations are carried out with the inclusion of burning particles, smoke, and oxidizer. The propellant mass loading is set at 17.6% aluminum. The droplets are injected with a zero initial velocity and are assumed to be in thermal equilibrium with the surrounding gas. The injected droplets have an initial composition of 90% aluminum, 10% oxide (a preformed oxide cap). The droplet properties are $\rho_{\text{Al}} = 1766$ kg/m$^3$, $c_{\text{Al}} = 1375$ J/(kgK); $\rho_{\text{ox}} = 1600$ kg/m$^3$, $c_{\text{ox}} = 1100$ J/(kgK).

Three aluminum distributions are studied: two skewed logarithmic distributions synthesized at distinct operating pressures, called distributions I and II (see Fig. 22), and a logarithmic normal distribution referred to as distribution III. The peak diameter for all three distributions is set to 30 $\mu$m. Smoke particles are assumed to be generated with a uniform diameter of 0.5 $\mu$m; the precise choice is not important provided it is much smaller than the droplet diameters.

Figure 23 shows the mixture spanwise-vorticity field, the mixture temperature, the particle locations (colored according to their diameters), and the smoke concentration at a representative time instant. The injection distribution I was used to obtain these results. It is observed that the flow has an unsteady behavior with large-scale vortices shedding from the shear layer and convecting in the rocket chamber before impinging on the nozzle wall. The particles are seen to fill the entire rocket chamber, and a total number of 110,000 are being continuously tracked. The aluminum droplets are strongly affected by the underlying gas field where they are spun away from the vortex centers; however, several large particles (red) are unaffected

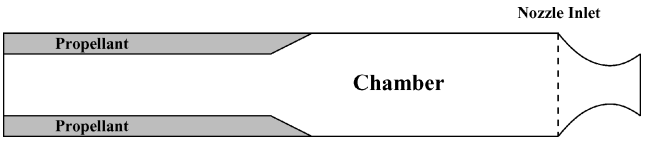


**Fig. 21 Schematic of model motor.**

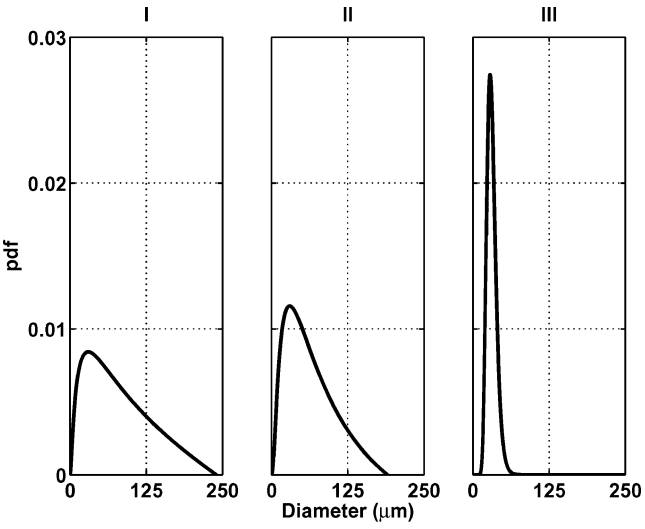


**Fig. 22 PDFs of the initial distributions for the chamber calculations. Compare I and II with the distribution of Fig. 12, and how they differ from the log-normal distribution III.**

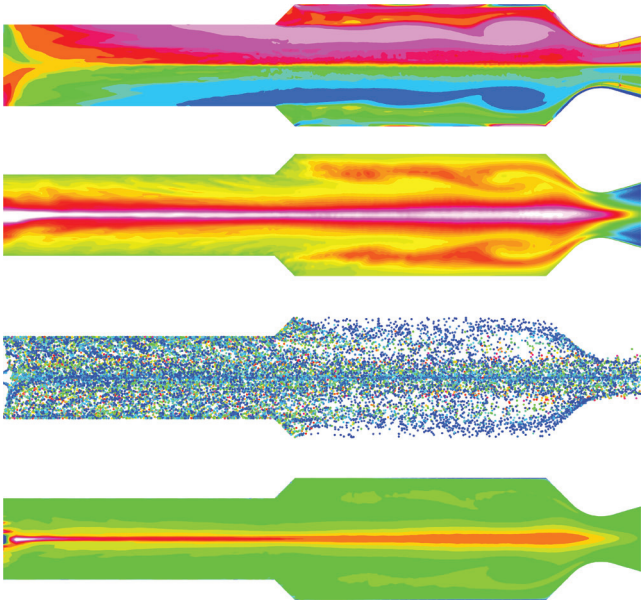

**Fig. 23 The mixture spanwise-vorticity field, the mixture temperature, the droplet locations (colored by their diameter size), and the smoke concentration at a representative time instant. Injection distribution I.**

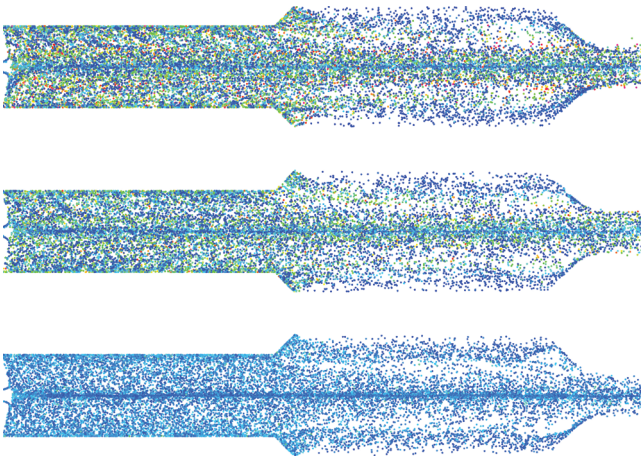

**Fig. 24 Particle locations obtained from the three injection distributions, I, II, and III, at the same time instant of the preceding figure.**

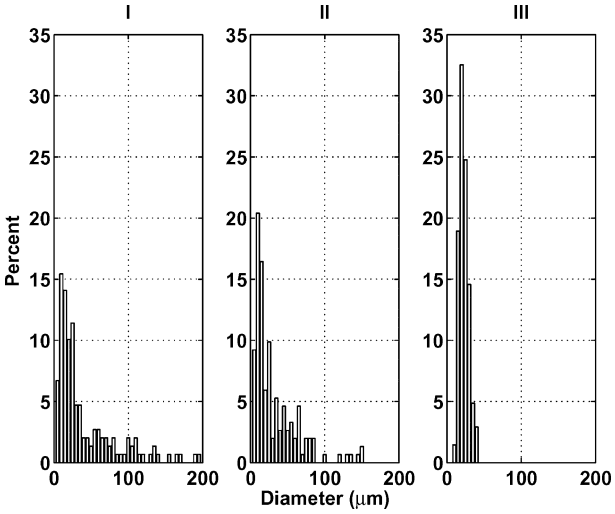


**Fig. 25 Instantaneous particle distributions at the nozzle entrance for the three initial distributions I (left), II (center), and III (right).**

by the structures as their momentum is high. Further, it is observed that the size distribution ranges from 1.5 to 240 $\mu$m; sizes smaller than the original distribution is because the particles are burning. Finally, the smoke concentration is low near the injecting walls and increases rapidly towards the core as expected.

Figure 24 shows the particle locations obtained from the three injection distributions, I, II, and III, at the same time instant of the preceding figure. The particles have been colored by diameter with blue (red) representing small (large) values. The coloring scheme between these figures is kept fixed to allow easier comparison. It is observed that the vortex cores and the shear layers have substantially fewer particles (as seen by the white area) while the droplets are evolving around these core regions. Comparing these three figures, the distributions for all three models appear to be qualitatively similar, although there seems to be a statistical variability.

To gain more insight, the histograms of the instantaneous size distribution at the nozzle inlet are plotted in Fig. 25. As can be seen from the figure, the histograms are significantly affected by the initial distributions. The histograms based on models I and II show a "richer" and wider size distribution than those based on the logarithmic normal distribution III. This observation highlights the fact that the agglomeration models proposed here can probably lead to more realistic distributions at the nozzle inlet than if a log-normal distribution were used. All previous numerical simulations found in the literature make use of either a single-size "representative" particle value or a logarithmic normal distribution. Here, the synthesis of the distributions obtained from the packing and agglomeration models permits computations to be performed that better mimic the real physics.

## V. Conclusions

The pocket model of Cohen,[7] although discredited as a quantitative predictive tool, identifies a crucial question: from what neighborhood do the particles in an agglomerate originate? It hypothesizes an answer to this question and in this way predicts the mean agglomerate diameter. Our strategy is the inverse of this: we examine experimental agglomerate data and calculate the neighborhood, assuming all that matters is proximity; and we have knowledge of proximity via packing models of the propellant morphology. Moreover, with the neighborhood known we predict the agglomerate distribution, a function of great practical importance.

Validation of our strategy lies in the comparison of the predicted distribution with experiment, and for such comparisons to be reliable the demands on the experimental data are high. They comprise the following:

1) A complete description of the propellant morphology statistics, including, most importantly, the aluminum distribution;

2) A description of the aluminum distribution leaving the surface is included. This should include all of the particles or, if only the agglomerates are included, a precise definition of this class (e.g., a specification of $\langle \text{cut} \rangle$);

3) The particles must be sampled close enough to the surface so that little consumption via combustion has occurred;

4) If mean diameters are identified, they must be defined.

Moreover, if the neighborhoods that we identify are, in due course, to be related to the detailed physics, validation will be aided by data that include the burning rate, the surface residence time of the particles, and information about the "walk" of a typical particle over the surface.

To our knowledge, there are no data that meet all of the requirements 1–4, but there are data that include enough information to justify tentative comparisons, and we have examined some of this here.

Distributions reported by Trubert[11] are reasonably predicted for 98% of the aluminum mass using model A, one for which proximity is characterized by a single parameter. When combustion between the propellant surface and the agglomerate collection point is accounted for, excellent agreement between theoretical and experimental number fraction distributions is obtained for all particles greater than 10 $\mu$m.

Data reported by Duterque[15] enable us to compare a distribution predicted by model A with the distributions predicted by model B, a two-parameter proximity model. This comparison is meaningful because the experimental data define one of these parameters. Agreement is good, which lends credence to model A, as model B is more clearly linked to key physics that controls agglomeration—surface residence time and surface mobility range.

Comparisons with data for the space shuttle booster propellant[16] are unsatisfactory. It is clear the experimental data are significantly affected by combustion.

Finally, data reported in Ref. 10 are used to give some indication of how the single model A parameter $S_d$ can vary with different propellants and different operating conditions.

The next step in this problem is to provide quantitative estimates of the proximity parameters using the physics of agglomeration. This would be best done in the context of model B or some variation of it. A full simulation, an extension of Rocfire,[2] is unlikely in the near future, but well-designed modeling strategies might be of value.

It is possible, for example, that Rocfire could be run to provide at any time a description of the AP surface topography, the map of the AP archipelago in the sea of binder; the output would also provide a description of the surface temperature of the binder. A separate code, two-dimensional, could then replace the binder by a liquid whose surface is the plane projection of the real binder, and which has a defined distribution of surface tension defined by the temperature variations. On this surface would be placed a disk, to represent a partly submerged aluminum drop, and the motion of this disk could perhaps be calculated, a Marangoni phenomenon. The motion of the disk would be irregular, ever changing because of the changing surface tension field, and constrained by the ever-changing boundaries between the binder and AP. Such calculations could provide statistical information about particle mobility, an ingredient of model B.

It is also possible that the numerical study of a single aluminum drop in molten binder could provide estimates of the residence time, the second ingredient of model B.

We hope to examine both of these problems in the coming months, but both have their challenges.

Our paper concludes, in Sec. IV, with an examination of the history of the aluminum between the time that it leaves the surface and the time that it arrives at the nozzle entrance. The description at the entrance is of particular interest to rocket designers. It is found that the logarithmic normal distribution, currently an industry standard, falls short on predicting the appropriate distribution at the nozzle entrance for model rockets. The distributions obtained from the random packs and agglomeration models can better provide the information needed to perform multiphysics computational-fluid-dynamics simulations.

## Acknowledgment

This work was supported by the U.S. Department of Energy through the University of California under Subcontract B341494. J. Buckmaster is also supported by the Air Force Office of Scientific Research. The authors would like to acknowledge J. Ferry, whose input during the course of this work was invaluable. In addition we are grateful to J. Trubert for supplying detailed data from his experimental paper on propellant 8061.

## References

[1]Price, E. W., and Sigman, R. K., "Combustion of Aluminized Solid Propellants," *Solid Propellant Chemistry, Combustion, and Motor Interior Ballistics*, edited by V. Yang, T. Brill, and W. Ren, Progress in Astronautics and Aeronautics, Vol. 185, AIAA, Reston, VA, 2000, pp. 663–688.

[2]Massa, L., Jackson, T. L., and Buckmaster, J., "New Kinetics for a Model of Heterogeneous Propellant Combustion," *Journal of Propulsion and Power* (to be published).

[3]Wang, X., Jackson, T. L., and Massa, L., "Numerical Simulation of Heterogeneous Propellant Combustion by a Level Set Method," *Combustion Theory and Modelling*, Vol. 8, No. 2, 2004, pp. 227–254.

[4]Wang, X., and Jackson, T. L., "The Numerical Simulation of Two-dimensional Aluminized Composite Solid Propellant Combustion," *Combustion Theory and Modelling* (to be published).

[5]Beckstead, M. W., "A Model for Solid Propellant Combustion," *14th Jannaf Combustion Meeting*, CPIA Publication 291, Vol. 1, Dec. 1977, pp. 281–306.

[6]Cohen, N. S., and Strand, L. D., "A Model for the Burning Rates of Composite Propellants," *17th JANNAF Combustion Meeting*, Vol. 1, Dec. 1980, pp. 53–97.

[7]Cohen, N. S., "A Pocket Model for Aluminum Agglomeration in Composite Propellants," *AIAA Journal*, Vol. 21, No. 3, 1983, pp. 720–725.

[8]Knott, G. M., Jackson, T. L., and Buckmaster, J., "The Random Packing of Heterogeneous Propellants," *AIAA Journal*, Vol. 39, No. 4, 2001, pp. 678–686.

[9]Kochevets, S., Buckmaster, J., Jackson, T. L., and Hegab, A., "Random Packs and Their Use in the Modeling of Heterogeneous Solid Propellant Combustion," *Journal of Propulsion and Power*, Vol. 17, No. 4, 2001, pp. 883–891.

[10]Sambamurthi, J. K., Price, E. W., and Sigman, R. K., "Aluminum Agglomeration in Solid-Propellant Combustion," *AIAA Journal*, Vol. 22, No. 8, 1984, pp. 1132–1138.

[11]Trubert, J. F., "Agglomeration and Combustion of Aluminum Particles in Solid Rocket Motors," Space Solid Propulsion, Paper 44, Nov. 2000.

[12]Hermsen, R. W., "Aluminum Combustion Efficiency in Solid Rocket Motors," AIAA Paper 81-0038, Jan. 1981.

[13]Brewster, M. Q., and Parry, D. L., "Radiative Heat Feedback in Aluminized Solid Propellant Combustion," *Journal of Thermophysics*, Vol. 2, No. 2, 1988, pp. 123–130.

[14]Bradley, E. G., and Brewster, M. Q., "Effect of Gas/Particle Coupling on Combustion Efficiency in Aluminized Solid Rockets," *Journal of Propulsion and Power*, Vol. 7, No. 6, 1991, pp. 1078–1080.

[15]Duterque, J., "Experimental Studies of Aluminum Agglomeration in Solid Rocket Motors," *4th International Symposium on Special Topics in Chemical Propulsion*, edited by K. K. Kuo, Begell House, New York, 1996, pp. 693–705.

[16]Laredo, D., McCrorie, J. D., II, Vaughn, J. K., and Netzer, D. W., "Motor and Plume Particle Size Measurements in Solid Propellant Micromotors," *Journal of Propulsion and Power*, Vol. 10, No. 3, 1994, pp. 410–418.

[17]Widener, J. F., and Beckstead, M. W., "Aluminum Combustion Modeling in Solid Propellant Combustion Products," AIAA Paper 98-3824, 1998.

[18]Ferry, J., and Balachandar, S., "Equilibrium Expansion for the Eulerian Velocity of Small Particles," *Powder Technology*, Vol. 125, Nos. 2–3, 2002, pp. 131–139.

[19]Najjar, F. M., Haselbacher, A., Ferry, J. P., Wasistho, B., Balachandar, S., and Moser, R. D., "Large Scale Multiphase Large-Eddy Simulation of Flows in Solid Rocket Motors," AIAA Paper 2003-3700, June 2003.

[20]Lupoglazoff, N., and Vuillot, F., "Parietal Vortex Shedding as a Cause of Instability for Long Solid Propellant Motors—Numerical Simulations and Comparisons with Firing Tests," AIAA Paper 96-0761, Jan. 1996.